Did deglaciation of the Greenland ice sheet cause a large earthquake and tsunami around 10,600 years ago?

R. Steffen[1,*], H. Steffen[1], R. Weiss[2], B. S. Lecavalier[3], G. A. Milne[4], Sarah A. Woodroffe[5], O. Bennike[6]

1 – Lantmäteriet, Lantmäterigatan 2, 80182 Gävle, Sweden

2 – Department of Geosciences, Virginia Tech, 4044 Derring Hall, Blacksburg, VA 24061, U.S.A.

3 – Department of Physics and Physical Oceanography, Memorial University of Newfoundland, St. John's, Newfoundland A1B 3X7, Canada

4 – Department of Earth Sciences, University of Ottawa, Marion Hall, 140 Louis Pasteur, Ottawa, Ontario K1N 6N5, Canada

5 – Department of Geography, Durham University, Lower Mountjoy, South Road, Durham, DH1 3LE, UK

6 – Geological Survey of Denmark and Greenland, Øster Voldgade 10, 1350 Copenhagen K, Denmark

*Corresponding author: rebekka.steffen@lm.se

Abstract

Due to their large mass, ice sheets induce large stresses in the Earth's crust. Stress release during deglaciation can trigger large-magnitude earthquakes, as indicated by surface faults in northern Europe. Here we show by the combined analysis of past sea level indicators and a model of glacially-triggered fault reactivation that deglaciation of the Greenland ice sheet may have caused a large magnitude earthquake around 10,600 years ago offshore south-western Greenland. If this stress release was dominated by a single event, it could have produced a tsunami in the North Atlantic Ocean with runup heights of up to 5 m in the British Isles and up to 6 m along Canadian coasts. As the Greenland Ice Sheet currently experiences substantial melting, a tsunami induced by a glacially-

triggered earthquake is a possibility for countries in the North Atlantic, which adds an additional climate-change related hazard to this region.

Introduction

The growth and decay of ice sheets during a glacial/interglacial cycle affect a multitude of processes on the surface as well as in the interior of the Earth. For example, the mass redistribution of water between the ice sheets and the oceans causes changes in the Earth's shape, gravity, rotation and sea level (1). This climate-driven surface loading results also in significant horizontal and vertical stress changes due to the enormous mass of the ice sheets (2, Fig. 1A). In a compressional stress setting, where horizontal stresses are larger than the vertical stress, fault slip and thus earthquake activity is inhibited (2), hence explaining the relatively low seismic activity in present-day Greenland (3). During deglaciation, however, the vertical stress decreases in relation to the vanishing ice, but the decrease of horizontal stresses is delayed due to bending of the lithosphere and the viscoelastic nature of the underlying mantle (2, 4), promoting fault reactivation in a compressional stress setting (Fig. 1B). Deglacial reactivation of faults has occurred in northern Europe, where more than a dozen glacially-induced faults (GIFs) have been identified, showing offsets of up to 30 m at the surface (5). They were created by earthquakes with moment magnitudes of up to 8.2 (6) during the deglaciation and shortly after. However, knowledge is limited for the currently glaciated regions of Greenland and Antarctica, even though Arvidsson (6) pointed to the possibility that future deglaciation of the ice sheets may cause large earthquakes. Although the Greenland Ice Sheet has exhibited accelerating mass loss over the past few decades (7), there is no evidence yet of a related increase in seismic activity (3, 8). Here, we take a different approach by considering the deglaciation of the ice sheet since the last glacial maximum around 20 ka before present (BP), during which the ice sheet lost ~40% of its mass (9, 10). We present the first calculations of stress changes induced by ice-mass loss in the early Holocene to assess whether and where glacially-triggered earthquakes were most likely to have occurred. Our modeling results indicate that southern Greenland is the most prone to glacially-induced faulting and

this is supported by sea-level reconstructions from geological records. Using a faulting scenario that is consistent with the geological records, we show that the modeled fault could have produced a tsunami wave (Fig. 1C) during the early Holocene, and we compute the wave height distribution around North Atlantic coasts.

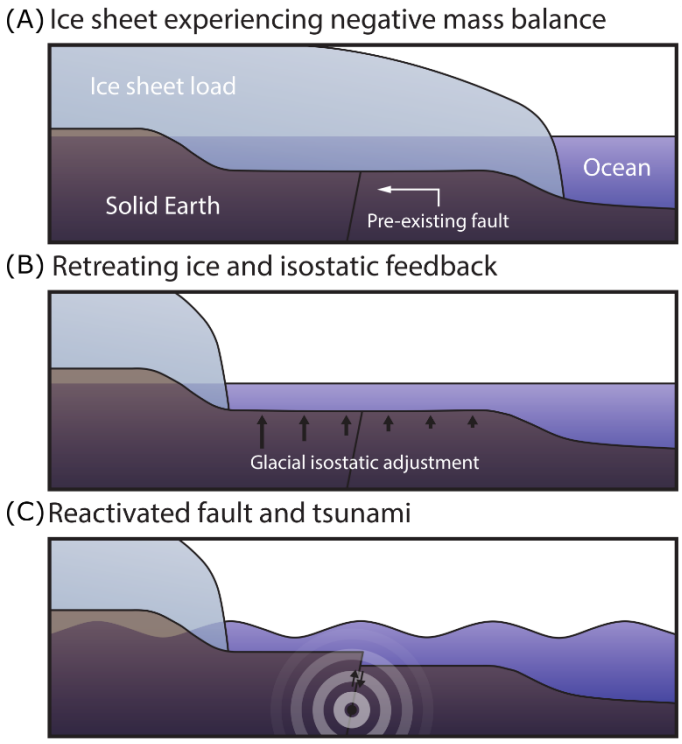

Figure 1: Stages of glacially-induced fault reactivation and tsunami development. (A) The ice sheet undergoes negative mass balance in response to climate warming. (B) Ice sheet retreat causes a viscoelastic glacial isostatic response from the solid Earth. (C) Due to an asynchronous decrease of horizontal and vertical stresses in a compressional stress setting, a pre-existing fault is reactivated triggering an earthquake and tsunami.

Results and Discussion

A recent model reconstruction of the Greenland Ice Sheet (termed Huy3; 9) and its appendant (optimal) Earth viscosity model (lithospheric thickness of 120 km, upper mantle viscosity of 5 * 10^{20} Pa*s, lower mantle viscosity of 2 * 10^{21} Pa*s) and ocean-load model are used to calculate stress changes during the past 120,000 years for the whole of Greenland in a compressional stress setting. Our modelling procedure follows the approach described in Wu (11) for a three-dimensional (3D) flat Earth approach.

Compressional stresses can be assumed due to ridge push east of Greenland at the Atlantic mid-ocean ridge towards the stable craton of North America to the west (12), which results in maximum east-

west horizontal stress and minimum north-south horizontal stress. This stress direction for Greenland is also confirmed by mantle flow models (13), which indicate a horizontal mantle movement for the area offshore southern Greenland. In addition, a horizontal direction of the maximum stress is inferred in the World Stress Map offshore of the north-east of the United States (14), and studies of the palaeostress direction in the Palaeocene show a rotation of the maximum horizontal stresses from north-south to east-west going from the north-eastern coast (Peary Land) to the south-eastern coast (Skjoldungen; 15). Stresses in the north–south direction are assumed to be small and similar in magnitude to vertical stresses; this is a reasonable assumption given the lack of active plate boundaries to the south and north of Greenland (12) and the observations of the palaeostresses along the eastern coast, which show a decrease of the intermediate stress magnitude from north to south (15).

Coulomb Failure Stress Changes

Assuming critically stressed conditions in the crust, which is valid for intraplate areas (16), we analyse the change in Coulomb Failure Stress ΔCFS (17) which helps visualize stable and unstable seismic conditions. Put simply, positive values of this quantity represent unstable conditions indicating that seismic activity is likely, and negative values point to stable conditions where seismic activity is unlikely. Only two areas, the southern tip and northern coast of Greenland, experience unstable conditions in the early Holocene due to negative ice-mass changes (Fig. 2, Movie S1).

Seismic activity within deglaciating regions requires pre-existing faults, which can be reactivated to release the deglaciation-related stress build-up (18). Faults in North Greenland are mainly striking east–west (90°/180°) while those in south-western Greenland, close to the small town of Nanortalik, mainly strike northwest–southeast (135°/315°) and northeast–southwest (45°/225°; 15, 19), although detailed regional fault parameters are lacking. ΔCFS calculations for various strike and dip values as well as stress ratios (20) show that faults with strike values of 90° cannot be reactivated in the chosen stress setting. Uenzelmann-Neben et al. (21) identified a fracture zone about 250 km to the south of Nanortalik, which shows disruptions of Pliocene sediment packages during the late Pleistocene. We

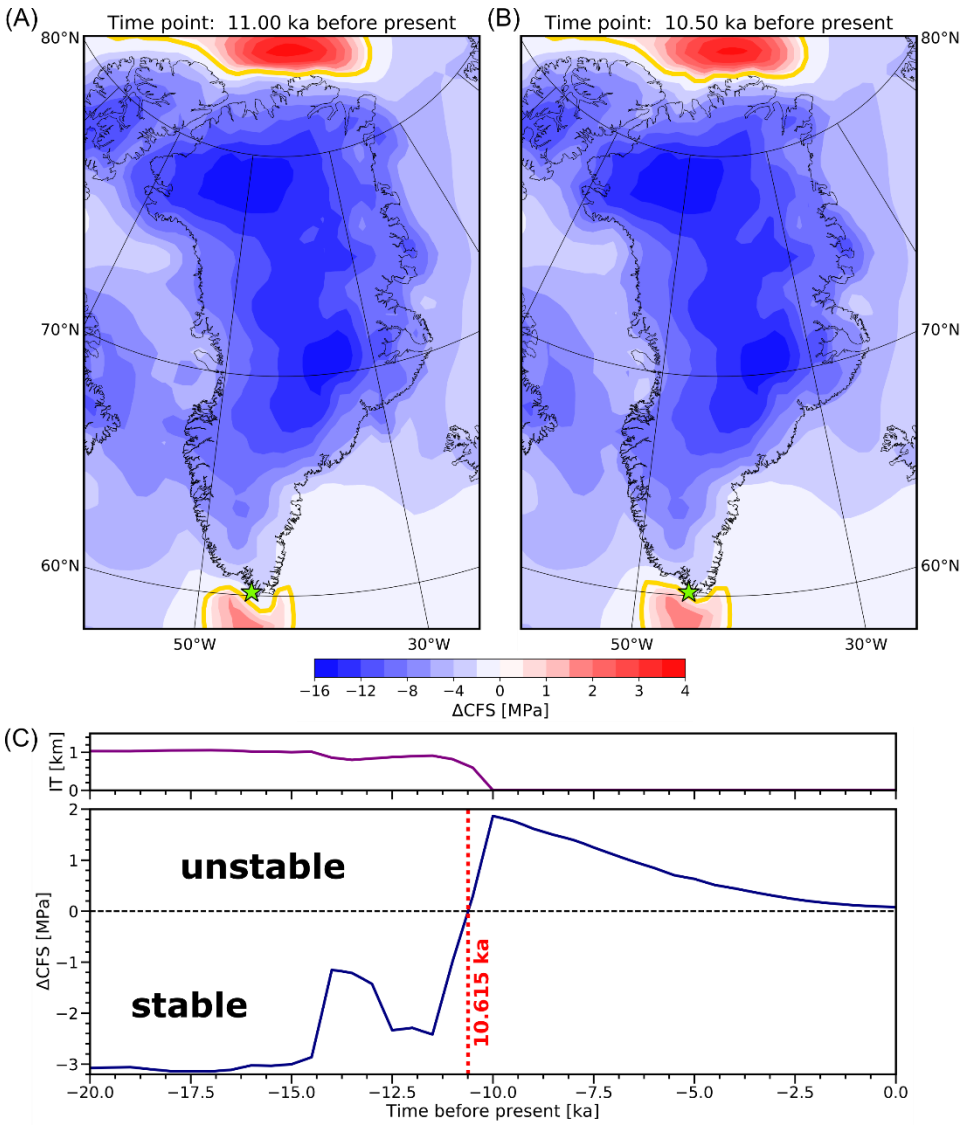

Figure 2: Stress variations for Greenland in the Holocene. The ΔCFS (Change in Coulomb Failure Stress) at 11 ka BP (A) and at 10.5 ka BP (B) is shown over Greenland. The yellow line marks the change from stable (blue) to unstable (red) conditions. (C) The ΔCFS over time for the last 20 ka for southern Greenland (green star in (A) & (B)). A potential fault with a dip of 45°, a strike of 315° and a coefficient of internal friction of 0.6 is assumed. The area becomes unstable at 10.615 ka BP (marked by red-dashed line). The ice thickness (IT) variation is shown on top as a purple line.

therefore focus on the south-western tip of Greenland, which becomes unstable at 10.615 ± 0.25 ka BP for our chosen model parameters (Fig. 2C). However, while glacially-triggered earthquakes in northern Europe have been identified using topographical changes and visible fault outcrops (5), such features have not yet been observed at the south-western tip of Greenland. Therefore, we look to observations of past relative sea-level (RSL) change to determine whether they are compatible with the timing and amplitude of faulting suggested by our model.

Evidence from the past

Several RSL data sets have been collected in the area around Nanortalik (Fig. 3) with sea-level indicators dating to 13.511 ± 0.236 ka BP (22), thus covering the time when the area is predicted to have become unstable (Fig. 2C). The applied deglaciation history Huy3, which results from the most recent analysis of this type and is based on a state-of-the-art ice extent and RSL database, shows first-order discrepancies to the RSL data from Nanortalik (Fig. 3C). The best-fitting models show a difference of 10.68 to 33.17 m for RSL data before 10.5 ka BP while for data after 10.5 ka BP the fit is excellent (Fig. 3C). The majority of RSL data around Greenland can be explained with the Huy3 model reconstruction (9). However, extensive changes to the ice model history (Greenland and North America) and Earth model parameters have been unable to resolve the first-order misfit to the four oldest data points at Nanortalik (9, 23). Specifically, an extensive parameter search was unable to fit the older (early Holocene) RSL data while maintaining a quality fit to RSL data in the Mid-to-Late Holocene. Even when using earth model parameters optimised to best fit data in southern Greenland (lithospheric thickness of 96 km, upper mantle viscosity of 3 * 1020 Pa*s, lower mantle viscosity of 3 * 1022 Pa*s) there remains a data-model discrepancy of up to 19 m. Two additional ice model reconstructions were considered (24, 25) but the model fits were of lower quality than those for the Huy3 model. One important boundary condition is the relatively narrow continental shelf adjacent to southern Greenland, which limits the maximum thickness of ice that can be simulated.

The RSL data from this location are of the highest quality – they are based on samples from isolation basins and show no sign of transport (22). Other factors that affect the timing and location of RSL markers, e.g. hard-water effects, marine and freshwater reservoir effects and contamination by older or younger carbon, can be therefore excluded. Other RSL data in the surrounding are younger than 10.54 ka and so cannot be used to test the possibility of glacially-induced faulting. Recent RSL data obtained from 10Be dating go back to 11.6 ka for the area close to the town Igaliku (26), which is around 100 km to the north of Nanortalik. A similar decrease in RSL to Nanortalik is observed, even though markers from 11.2 ka have been found at 44.8 and 19.1 m above modern sea level.

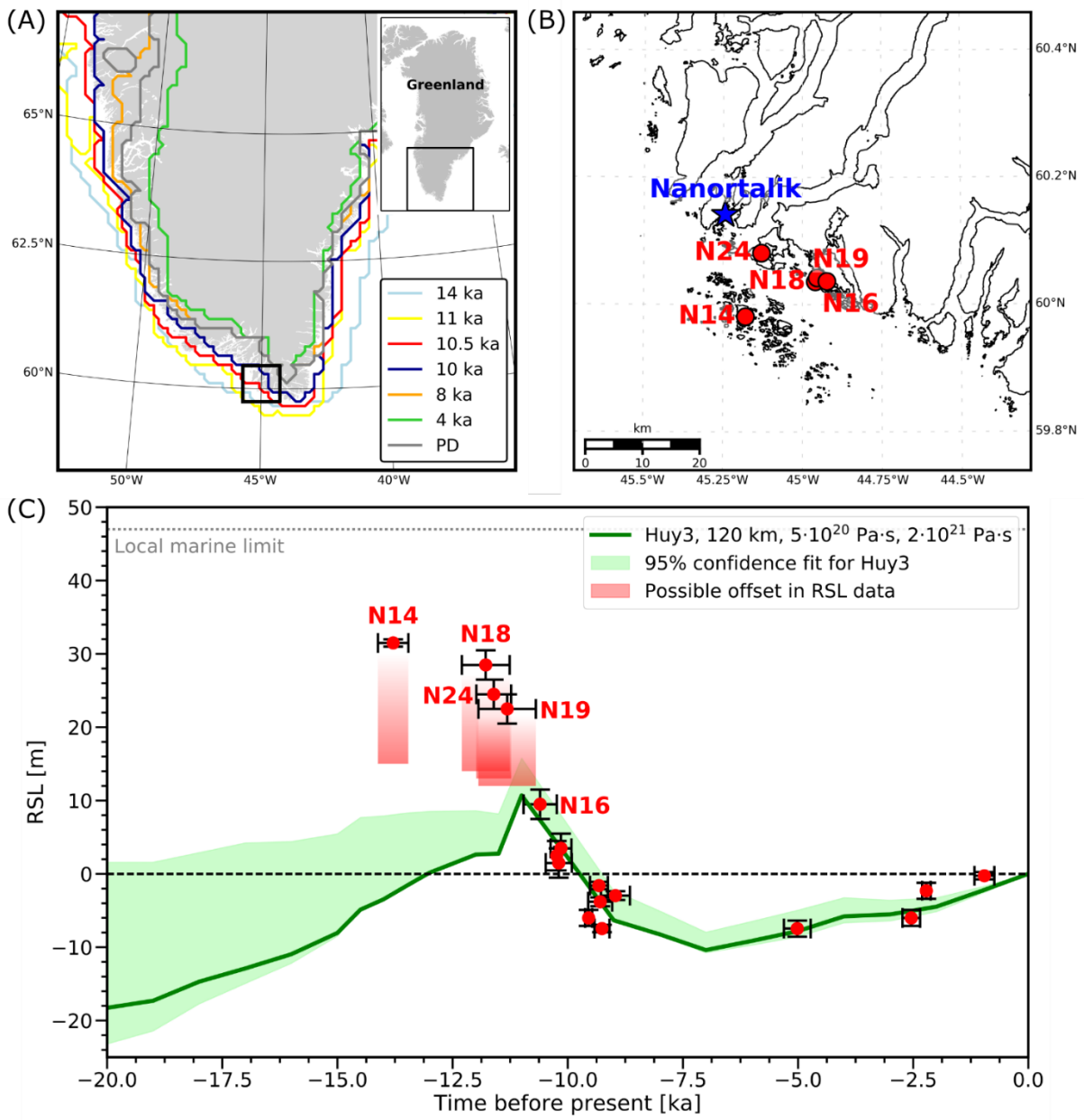

Figure 3: Ice-sheet extent variations in southern Greenland and relative-sea level observations at Nanortalik. (A) Boundaries of the ice model Huy3 (9) for different times (PD = present day). Black rectangle shows area in (B). (B) Location of RSL observations and the town of Nanortalik. (C) RSL observations and predictions using Huy3. The green line is obtained from the best-fitting Earth model with a lighter green bounding envelop based on RSL curves using the nominal 95% confidence interval Earth models (described in Table 2 of Lecavalier et al. (9)). The RSL observations are shown with 2-σ uncertainty in the time and height range as black bars. The maximum possible offset to allow a better to fit to the RSL predictions as well as to have an RSL fall only are shown as red squares for N14, N18, N19 and N24.

Based on our results above, we propose the hypothesis that tectonic activity led to the movement of RSL markers older than ~10.6 ka. The occurrence of such an event would influence the elevation of RSL markers older than this age but not younger ones, thus resolving the previously noted data-model discrepancies (Fig. 3C), which we explore next. The isolation basin at N16 (Fig. 3) has an inferred age of 10.6 ka BP and the excellent fit to RSL predictions indicates that this basin was not affected by an

earthquake, providing a further time constraint. In addition, as the sediments in the isolation basins N14, N18, N19 and N24 show no sign of sea-level rise, a maximum correction of up to 16.5 m can be assumed (Fig. 3C, red boxes). Invoking a faulting event allows the possibility to have only RSL fall, but also to increase the fit between RSL curve predictions and faulting-corrected RSL heights.

Fault Modelling

To simulate an earthquake due to the modelled stress changes, we created a two-dimensional (2D) GIA (Glacial Isostatic Adjustment)-fault model (18) and considered a range of plausible fault parameters (e.g. fault depth, fault width, friction). As discussed above, the tectonic regime in southern Greenland indicates that deglaciation would most likely result in thrust faulting with a strike orientation that is NW-SE (or SE-NW). Of all the faults we considered, via a set of parameter values for dip, depth, strike and friction, the one described below is the most likely to have been reactivated based on the offsets indicated by the RSL data. The modelled offshore thrust fault southwest of Nanortalik (Fig. 4A) results in a surface deformation that uplifts all RSL data points older than 10.6 ka in the area. This fault has a dip of 45° and extends from a depth of 5 km to 24 km and hence does not outcrop at the surface; its strike is parallel to the outer coast at 315° and thus parallel to faults identified in this area.

In our model, the fault is reactivated at 10.615±0.25 ka BP with a fault slip of 43.7 m, equivalent to an earthquake with a moment magnitude of about 8.4 using a fault length of 250 km. This moment magnitude is larger compared to estimates for other GIFs, but those previous estimates are based on fault offsets visible at the surface and slip within the crust was most likely larger due to the increase in displacement towards the fault centre (e.g., 27). An earthquake with such a large magnitude is rare and usually occurs along active, convergent, plate boundaries rather than the intraplate setting considered here. On a related note, recent results by Smith et al. (28) showed that offsets along GIFs in northern Sweden were not created in one event but rather two or more events. Assuming a similar scenario here with several earthquakes that created a total fault slip of 47.3 m along a 250 km long

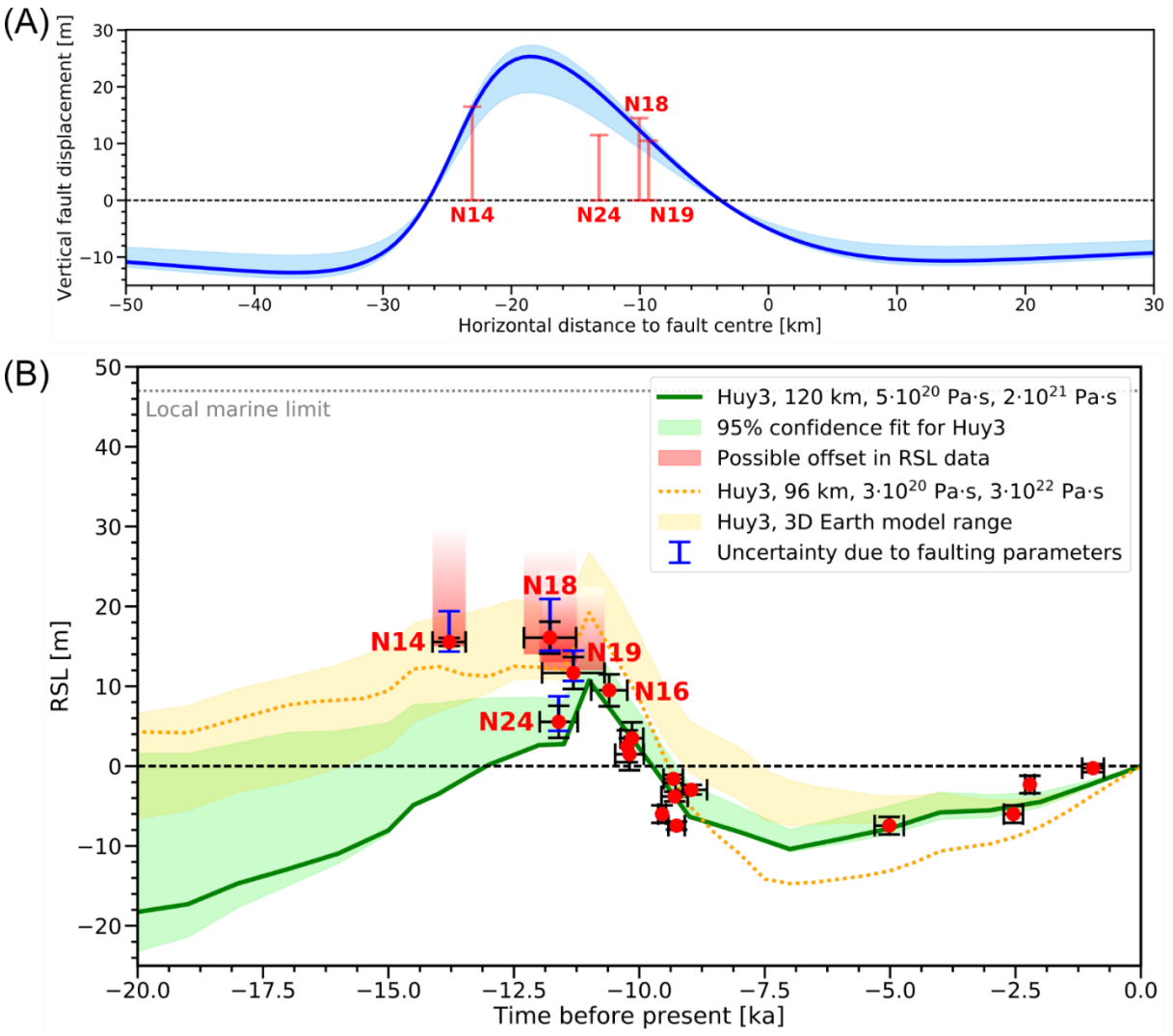

Figure 4: Vertical fault displacement and estimated corrections for the RSL points. The vertical fault displacement is obtained for a fault dipping at 45° and extending between 5 and 24 km depth. Results are based on values of 0.6 and 0.12 for static and steady-state friction, respectively. (A) Vertical displacement vs. horizontal distance to fault center projected on the model Earth surface with parametric uncertainty (light-blue) associated with using a steady-state coefficient of friction between 0.06 and 0.18 and different rupture times. RSL heights with maximum possible offset are shown in red. (B) Modified RSL curve for Nanortalik considering the correction of the RSL observations by the obtained vertical fault displacement. The blue bars mark the uncertainty associated with parametric uncertainty from the fault modelling (light-blue area shown in (A)). A range of RSL curve predictions using various 3D Earth models (yellow area) as well as the best-fitting Earth model for southern Greenland (dashed yellow line) indicate the range of further RSL curves (after Milne et al. (23)).

fault, the moment magnitude could be reduced to 7.7 for ten earthquakes with slips of 4.73 m each. An additional possibility is a decrease of the fault length to 100 km with ten slips of 4.73 m resulting in much smaller moment magnitudes of 5.8 for each earthquake, which is more commonly observed for intraplate earthquakes (e.g., (29)).

Even though the strike direction of the fault (315°) is similar to that of faults observed in the Nanortalik region, this specific fault has not (yet) been identified, which may be due to the location of the fault being offshore and the lack of high-quality, high-resolution seismic data (21). We note that our

calculations neglect the influence of pore-fluid pressure as no information is available on how this parameter changes in a crustal setting beneath the ice.

The vertical displacement at the surface induced by this modelled earthquake would increase the elevation of RSL observations older than 10.6 ka by 10.8 to 19.0 m (Fig. 4A). These displacements move the observations closer to the best-fitting modelled sea-level curve and effectively resolve the data-model discrepancies. The data are now mostly at the bottom of the indicated RSL correction and are within possible 3D Earth model fits using Huy3 (Fig. 4B). The mismatch to the best fitting curve for southern Greenland is also now decreased. However, one data point, N24, is too low, indicating that the fault movement is excessive (Fig. 4B). This includes the parametric uncertainties associated with the 2D fault model as well as the unmodelled slip dependency along the fault in the strike direction. Fault slip models of previous large earthquakes show strong lateral variations along strike (e.g., 27), which have not been modelled here. A change in the vertical displacement based on a smaller fault slip magnitude could decrease the fault offset by up to 25% over a short distance of only 10 to 15 km. The location of the RSL marker N24 is displaced around 15 km along strike relative to the other RSL data. This could lead to a decrease of the fault offset from 19.0 m to 14.25 m, moving the N24 marker up again and within the range of possible GIA model runs (Fig. 4B). In addition, local variations in the geology and a system of faults rather than just one fault could lead to slightly different fault displacements and enhance (or reduce) the quality of fit. However, this cannot be solved using the homogeneous Earth models applied here and so is a target for future research.

Geomorphological evidence for GIFs in Greenland has not been observed to date but this is mainly due to the fact that GIFs have not been considered for this region. GIFs in northern Europe have been mainly identified by visible offsets at the surface and, in more recent years, via soft-sediment structures or high-resolution elevation data. Bathymetric data for southwestern Greenland have poor resolution and so a gradient of less than 4.5 m/km as obtained from the predicted vertical fault displacement at the surface (Fig. 4A) would be difficult to identify. The optimum vertical fault displacement is also related to a maximum offset in RSL data, and so a more rapid RSL fall associated

with GIA would require a smaller fault slip. Nevertheless, the misfit between RSL observations and GIA model output as well as the timing and location of predicted unstable conditions provide support for the occurrence of tectonic activity in this area in the early Holocene. As RSL data are crucial constraints for ice model calibrations we suggest that RSL data proximal to ice sheets should be investigated for fault offsets due to ice retreat, otherwise glaciological simulations might be biased in certain regions of interest, e.g., Greenland, the Canadian Arctic and the Barents Sea.

The southern tip of Greenland is an area of high seismicity compared to other parts of Greenland (30), but magnitudes are mostly below 3.0, which is similar to the ones observed at the Pärvie fault in Fennoscandia (31). In addition, Voss et al. (30) noted that many more earthquakes can be expected, if the station density is increased (currently only two stations) and the magnitude of completeness could be decreased to below 3. Therefore, previous moderate to large magnitude seismicity is a possibility. However, the current observations in southern Greenland allow no differentiation between one-large magnitude event vs a series of smaller events with magnitudes in the range of 6 to almost 8. Thus, neither only one nor several earthquakes can be excluded, and further field observations are necessary (e.g., fault mapping, fault dating) to identify and constrain the occurrence of seismic activity during the early Holocene.

Tsunami generation

Vertical displacement of the sea floor can produce tsunami waves. We use the slip distribution of the 2D model, the modern-day bathymetry of the Atlantic Ocean and assume that stress was released in a single event to evaluate if a significant tsunami could have been created by the modelled earthquake that is most compatible with the RSL observations. The obtained 2D fault slip is interpolated to a 3D distribution towards the edges of the fault (Fig. 5A) and the sea-level has been decreased by 35.2 m, which is the eustatic sea-level of Huy3 at 10.615 ka.

Based on the simulated earthquake characteristics, our results suggest a sizable tsunami that impacted the shorelines of North America and Europe (Fig. 5B). Greenland experienced the largest tsunami

waves (generally exceeding 1.5 m with a maximum of 7.2 m at the southern tip). Tsunami waves of up to 1.5 m in amplitude reached North America (Fig. 5B), while those reaching Europe exhibit maximum tsunami elevations between 0.5 and 1.2 m (Fig. 5B). Note that these maxima are retrieved from the simulations in 50-m water depth and the tsunami waves experience further increase of wave elevation as they approach the shore. This process is known as shoaling and causes the tsunami-wave amplitude to grow by a factor between 4 and 6 (32), resulting in a maximum runup of about 7.5 m and 6 m along North American and European coasts, respectively. Tides were not considered in our simulations; however, they can be important as the tidal range in the North Atlantic can exceed 1 m (33) and can grow to macrotidal conditions in some estuaries and inlets (e.g., Bay of Fundy).

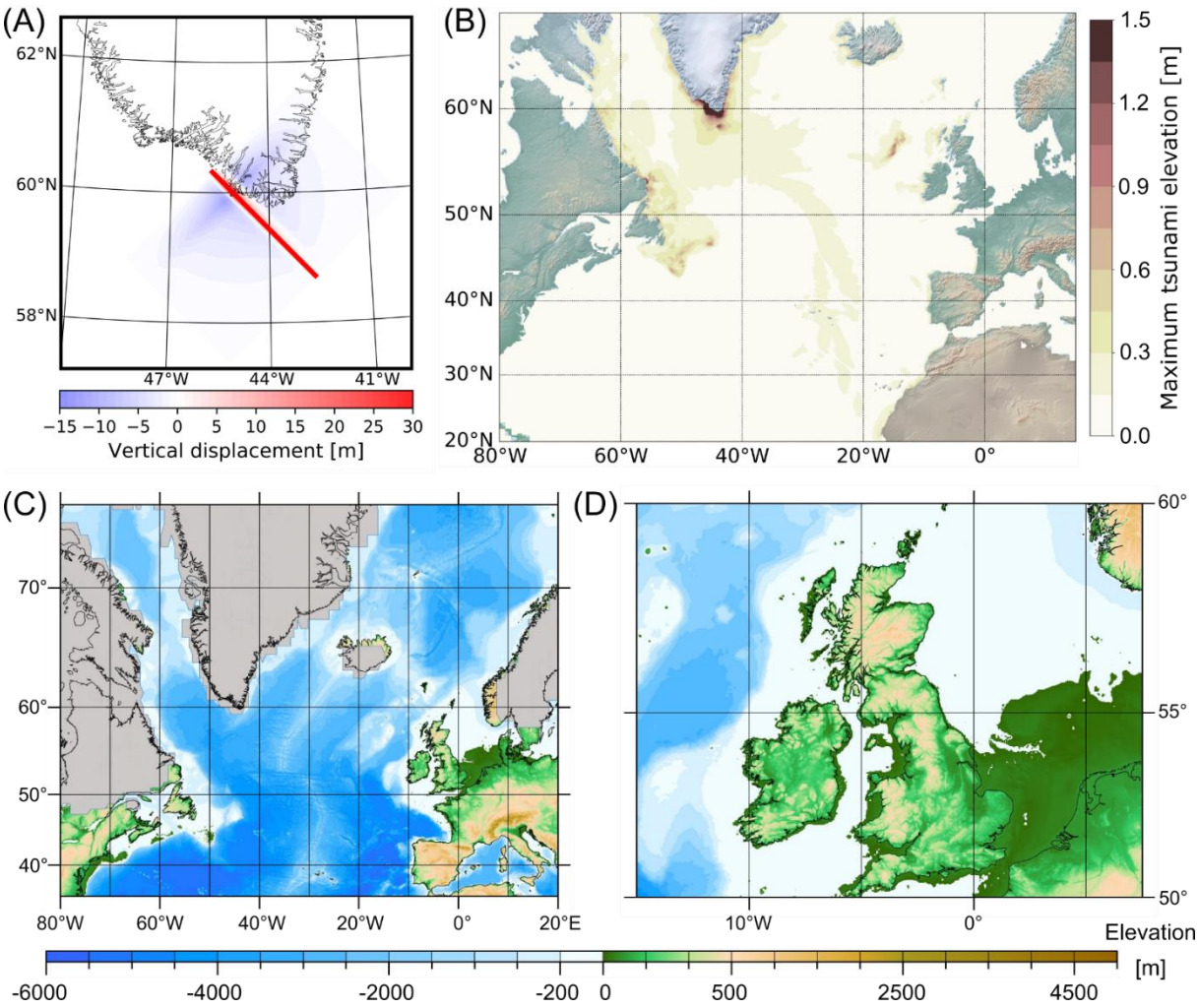

Figure 5: Fault displacement and their corresponding tsunami deep-water wave amplitude as well as paleogeographic overview of the North Atlantic region. (A) Vertical fault displacement interpolated to the edges of the fault trace for a fault length of 250 km. (B) The distribution of the deep-water wave amplitude over the entire North Atlantic. Paleogeography and ice-sheet distribution (grey) of the North Atlantic region (C) as well as for the western European coast (D).

Tsunami deposits related to the offshore Nanortalik earthquake have not been identified. One problem in finding tsunami deposits on Greenland is that only very few sedimentary environments, such as coastal lakes, were ice free by 10.6 ka BP (34). The area of Nanortalik was mainly ice covered until 10.5 ka ago (Fig. 3A, 5C) and the fault was most likely reactivated at the boundary of the ice sheet. The coasts of Newfoundland and the Gulf of St. Lawrence were ice free (35), but grounded ice extended to the present-day coastline of Labrador (36, 37) and Iceland. This would have prevented the deposition of tsunami deposits. A recent catalogue of RSL data for the eastern Canadian coastline shows a data gap between 13 ka and 7 ka along the north-eastern coast of Newfoundland (37), indicating the lack of evidence for a tsunami in the early Holocene. An additional factor is that sea level was considerably lower (several 10s of meters) in most ice-free areas of the North Atlanic around 10.6 ka (Fig. 5C). The Irish and British coasts, for example, were further to the west and deposits would be located offshore at present. In addition, the report by O'Brien et al. (38) lists recent storm and tsunami events along the Irish coast but points out that several events that occurred in the past might have been missed. The later occurring Storegga tsunami (around 8 ka BP; 39) could have also washed out earlier deposits from the Nanortalik tsunami. Tsunami deposits related to the Storegga landslide have only been documented at a single location in East Greenland (39) showing the difficulties in finding such deposits. In addition, the interaction of tsunami waves with sea ice in coastal areas decreases the tsunami impact significantly. Therefore, it might not be possible to find tsunami deposits that can be related to our modelled Nanortalik earthquake. Nevertheless, given that the predicted fault occurred offshore, the potential generation of a tsunami is high and thus offers an additional avenue to test our hypothesis. This also brings in an important element of natural hazard given the ongoing melting ice sheet that is relevant to countries bordering the North Atlantic.

Conclusion

The release of glacially-induced stresses leads to the prediction of earthquakes as has been recorded in parts of northern Europe from geological evidence. Here we propose the occurrence of glacially-

induced faulting offshore Nanortalik (south-western tip of Greenland) in the early Holocene based on stress modelling and the difficulty in simulating the large and rapid RSL fall in this region as recorded in high-precision geological records. The stress release could have been associated with a single, 8.2 magnitude event or a series of moderate to strong magnitude earthquakes. If the stress release was dominated by a single event, there are implications for tsunami generation (Fig. 1); with preliminary model simulations indicating that run-up heights of several metres are possible along eastern and western North Atlantic coasts. This adds a previously neglected future danger for countries bordering the North Atlantic as the current and projected ice-mass loss in Greenland over the coming decades is close to that experienced during the early Holocene. However, poor knowledge about offshore and onshore faults on and around Greenland limits our ability to make accurate predictions of which are most likely to be reactivated.

References

1. P. Wu, W.R. Peltier, Viscous gravitational relaxation. *Geophysical Journal of the Royal Astronomical Society* **70**, 435-485 (1982). doi:10.1111/j.1365-246X.1982.tb04976.x
2. A.C. Johnston, Suppression of earthquakes by large continental ice sheets. *Nature* **330**, 467-469 (1987). doi:10.1038/330467a0
3. P. Voss, S. Kildegaard Poulsen, S. Simonsen, S. Gregersen, Seismic hazard assessment of Greenland. *Geological Survey of Denmark and Greenland Bulletin Bulletin* **13**, 57–60 (2007).
4. P. Wu, H.S. Hasegawa, Induced stresses and fault potential in eastern Canada due to a disc load: a preliminary analysis. *Geophysical Journal International* **127**, 215–229 (1996). doi: 10.1111/j.1365-246X.1996.tb01546.x
5. R. Lagerbäck, M. Sundh, Early Holocene faulting and paleoseismicity in Northern Sweden. *Sveriges geologiska undersökning*, Research paper C **836**, 84 p. (2008).
6. R. Arvidsson, Fennoscandian Earthquakes: Whole Crustal Rupturing Related to Postglacial Rebound. *Science* **274**, 744-746 (1996). doi:10.1126/science.274.5288.744

7. M. McMillan, A. Leeson, A. Shepherd, K. Briggs, T.W.K. Armitage, A. Hogg, P. Kuipers Munneke, M. van den Broeke, B. Noël, W.J. van de Berg, S. Ligtenberg, M. Horwath, A. Groh, A. Muir, L. Gilbert, A high-resolution record of Greenland mass balance. *Geophysical Research Letters* **43**, 7002–7010 (2016). doi:10.1002/2016GL069666
8. M. Olivieri, G. Spada, Ice melting and earthquake suppression in Greenland. *Polar Science* **9**, 94-106 (2015). doi:10.1016/j.polar.2014.09.004
9. B.S. Lecavalier, G.A. Milne, M.J.R. Simpson, L. Wake, P. Huybrechts, L. Tarasov, K.K. Kjeldsen, S. Funder, A.J. Long, S. Woodroffe, A.S. Dyke, N.K. Larsen, A model of Greenland ice sheet deglaciation constrained by observations of relative sea level and ice extent. *Quaternary Science Reviews* **102**, 54-84 (2014). doi:10.1016/j.quascirev.2014.07.018
10. S.A. Khan, I. Sasgen, M. Bevis, T. van Dam, J.L. Bamber, J. Wahr, M. Willis, K.H. Kjær, B. Wouters, V. Helm, B. Csatho, K. Fleming, A.A. Bjørk, A. Aschwanden, P. Knudsen, P. Kuipers Munneke, Geodetic measurements reveal similarities between post–Last Glacial Maximum and present-day mass loss from the Greenland ice sheet. *Science Advances* **2**, e1600931 (2016). doi:10.1126/sciadv.1600931
11. P. Wu, Using commercial finite element packages for the study of earth deformations, sea levels and the state of stress. *Geophysical Journal International* **158**, 401-408 (2004). doi:10.1111/j.1365-246X.2004.02338.x
12. P. Bird, An updated digital model of plate boundaries. *Geochemistry, Geophysics, Geosystems* **4**, 1027 (2003). doi:10.1029/2001GC000252
13. C.P. Conrad, M.D. Behn, Constraints on lithosphere net rotation and asthenospheric viscosity from global mantle flow models and seismic anisotropy. *Geochemistry, Geophysics, Geosystems* **11**, Q05W05 (2010). doi:10.1029/2009GC002970
14. O. Heidbacha M. Rajabi, X. Cui, K. Fuchs, B. Müller, J. Reinecker, K. Reiter, M. Tingay, F. Wenzel, F. Xie, M.O. Ziegler, M.-L. Zoback, M. Zoback, The World Stress Map database

release 2016: Crustal stress pattern across scales. *Tectonophysics* **744**, 484-498 (2018). doi:10.1016/j.tecto.2018.07.007

15. P. Guarnieri, Pre-break-up palaeostress state along the East Greenland margin. *Journal of the Geological Society* **172**, 727-739 (2015). doi:10.1144/jgs2015-053
16. M.D. Zoback, J. Townend, Implications of hydrostatic pore pressures and high crustal strength for the deformation of intraplate lithosphere. *Tectonophysics* **336**, 19-30 (2001). doi:10.1016/S0040-1951(01)00091-9
17. R.A. Harris, Introduction to Special Section: Stress Triggers, Stress Shadows, and Implications for Seismic Hazard. *Journal of Geophysical Research* **103**, 24347-24358 (1998). doi:10.1029/98JB01576
18. R. Steffen, P. Wu, H. Steffen, D.W. Eaton, On the implementation of faults in finite-element glacial isostatic adjustment models. *Computers & Geosciences* **62**, 150-159 (2014). doi:10.1016/j.cageo.2013.06.012
19. N. Henriksen, A.K. Higgins, F. Kalsbeek, T.C.R. Pulvertaft, Greenland from Archean to Quaternary. *Geological Survey of Denmark and Greenland Bulletin Bulletin* **18**, 126 p. (2009).
20. J.W. Gephart, D.W. Forsyth, An improved method for determining the regional stress tensor using earthquake focal mechanism data: Application to the San Fernando Earthquake Sequence. *Journal of Geophysical Research* **89**, 9305–9320 (1984). doi:10.1029/JB089iB11p09305
21. G. Uenzelmann-Neben, D.N. Schmidt, F. Niessen, R. Stein, Intraplate volcanism off South Greenland: caused by glacial rebound? *Geophysical Journal International* **190**, 1–7 (2012). doi:10.1111/j.1365-246X.2012.05468.x
22. O. Bennike, S. Björck, K. Lambeck, Estimates of South Greenland late-glacial ice limits from a new relative sea level curve. *Earth and Planetary Science Letters* **197**, 171–186 (2002). doi:10.1016/S0012-821X(02)00478-8

23. G.A. Milne, K. Latychev, A. Schaeffer, J.W. Crowley, B.S. Lecavalier, A. Audette, The influence of lateral Earth structure on glacial isostatic adjustment in Greenland. *Geophysical Journal International* **214**, 1252-1266 (2018). doi:10.1093/gji/ggy189

24. W.R. Peltier, Global glacial isostasy and the surface of the ice-age Earth: The ICE-5G (VM2) model and GRACE. *Annual Review of Earth and Planetary Sciences* **32**, 111-149 (2004). doi:10.1146/annurev.earth.32.082503.144359

25. K. Fleming, K. Lambeck, Constraints on the Greenland Ice Sheet since the Last Glacial Maximum from sea-level observations and glacial-rebound models. *Quaternary Science Reviews* **23**, 1053–1077 (2004). doi:10.1016/j.quascirev.2003.11.001

26. P.R. Bierman, J. Shakun, E. Portenga, D. Rood, L.B. Corbett, Directly dating post-glacial Greenlandic emergence at high resolution using in situ 10Be. *Quaternary Research* **90**, 110-126 (2018). doi:10.1017/qua.2018.6

27. T. Kobayashi, Y. Morishita, H. Yarai, Detailed crustal deformation and fault rupture of the 2015 Gorkha earthquake, Nepal, revealed from ScanSAR-based interferograms of ALOS-2. *Earth, Planets and Space* **67**, 201 (2015). doi:10.1186/s40623-015-0359-z

28. C.A. Smith, S. Grigull, H. Mikko, Geomorphic evidence of multiple surface ruptures of the Merasjärvi “postglacial fault”, northern Sweden. *GFF* **140**, 318-322 (2018). doi:10.1080/11035897.2018.1492963

29. W.D. Mooney, J. Ritsema, Y.K. Hwang, Crustal seismicity and the earthquake catalog maximum moment magnitude (M_{cmax}) in stable continental regions (SCRs): Correlation with the seismic velocity of the lithosphere. *Earth and Planetary Science Letters* **357-358**, 78-83 (2012). doi:10.1016/j.epsl.2012.08.032

30. P.H. Voss, T.B. Larsen, T. Dahl-Jensen, Earthquakes in Greenland – a review. Abstract ESC2016-220 presented at the 35th General Assembly of the European Seismological Commission, Trieste, Italy, 4-10 September (2016).

31. E. Lindblom, B. Lund, A. Tryggvason, M. Uski, R. Bödvarssson, C. Juhlin, R. Roberts, Microearthquakes illuminate the deep structure of the endglacial Pärvie fault, northern Sweden. *Geophysical Journal International* **201**, 1704-1716 (2015). doi:10.1093/gji/ggv112
32. C.E. Synolakis, Green's law and the evolution of solitary waves. *Physics of Fluids A: Fluid Dynamics* **3**, 490 (1991). doi:10.1063/1.858107
33. O.B. Andersen, Ocean tides in the northern North Atlantic and adjacent seas from ERS 1 altimetry. *Journal of Geophysical Research* **99**, 22557-22573 (1994). doi:10.1029/94JC01433
34. S. Funder, K.K. Kjeldsen, K.H. Kjær, C.Ó. Cofaigh, The Greenland ice sheet during the past 300,000 years. A review, in J. Ehlers, P.L. Gibbard, P.D. Hughes, eds., *Quaternary Glaciations – Extent and Chronology: Developments in Quaternary Science* **15**, 699-713 (2011). doi:10.1016/B978-0-444-53447-7.00050-7
35. A.S. Dyke, An outline of North American deglaciation with emphasis on central and northern Canada. In J. Ehlers, P.L. Gibbard, eds., *Quaternary Glaciations – Extent and Chronology: Part II: North America: Developments in Quaternary Science* **2**, 373-424 (2004). doi:10.1016/S1571-0866(04)80209-4
36. L. Tarasov, A.S. Dyke, R.M. Neal, W.R. Peltier, A data-calibrated distribution of deglacial chronologies for the North American ice complex from glaciological modelling. *Earth and Planetary Science Letters* **315–316**, 30–40 (2012). doi:10.1016/j.epsl.2011.09.010
37. M. Vacchi, S.E. Engelhart, D. Nikitina, E.L. Ashe, W.R. Peltier, K. Roy, R.E. Kopp, B.P. Horton, Postglacial relative sea-level histories along the eastern Canadian coastline. *Quaternary Science Reviews* **201**, 124-146 (2018). doi:10.1016/j.quascirev.2018.09.043
38. L. O'Brien, E. Renzi, J.M. Dudley, C. Clancy, F. Dias, Catalogue of extreme wave events in Ireland: revised and updated for 14 680 BP to 2017. *Natural Hazards and Earth System Sciences* **18**, 729–758 (2018). doi:10.5194/nhess-18-729-2018

39. B. Wagner, O. Bennike, M. Klug, H. Cremer, First indication of Storegga tsunami deposits from East Greenland. *Journal of Quaternary Science* **22**, 321-325 (2006). doi:10.1002/jqs.1064